Oxidation of a 2wt.%Hf–doped (Ta,C)-rich nickel–based alloy between 1100 and 1250°C

Patrice Berthod, Dame Assane Kane, Lionel Aranda

RESEARCH ARTICLE

Asian Research Association

BULLETIN OF SCIENTIFIC RESEARCH

DOI: 10.54392/bsr2224

Oxidation of a 2wt.%Hf–doped (Ta,C)-rich nickel–based alloy between 1100 and 1250°C

P. Berthod [a,*], D.A. Kane [b], L. Aranda [a]

[a] Institut Jean Lamour, Université de Lorraine, Nancy, 54000, France
[b] Faculté des Sciences and Technologies, Université de Lorraine, Vandoeuvre-lès-Nancy, 54500, France
*Corresponding author Ph: (+33) 372742729 E-mail: patrice.berthod@univ-lorraine.fr
DOI: https://doi.org/10.54392/bsr2224
Received: 07-09-2022 ; Accepted: 16-11-2022 ; Published: 19-11-2022

Abstract: In this work, an alloy based on nickel, rich in chromium and designed to be reinforced by MC carbides thanks to the presence of 4wt.% Ta and 2wt.% Hf, was elaborated by conventional casting and exposed to air at three temperatures ranging from 1100 to 1250°C, with follow up of the mass changes due to oxidation. The as–cast microstructure is composed of a dendritic matrix and of eutectic carbides of two types. The major type is (Ta,Hf)C carbide and a minor type is chromium carbide. The isothermal mass gains are slow and their kinetics are of a parabolic type at all temperatures. The alloy demonstrated a chromia–forming behavior in all cases, with the development of an external continuous chromia scale and an internal layer of complex oxide $Cr(Ta,Hf)O_4$. The stability of the external scale during cooling was dependent on the quantity of oxides isothermally formed, i.e. on the oxidation temperature for a given duration. The behavior of the alloy in isothermal oxidation at the considered temperatures is satisfactory but solutions must be found for improving the resistance against cyclic oxidation for the highest temperatures.

Keywords: Nickel-based alloy, Hf-doping, Thermal analysis, High temperature oxidation, Metallographic characterization

1. Introduction

Pieces made of superalloys working at elevated temperatures in various industrial and transportation systems are often subjected to mechanical stresses and chemical aggressivity from the hot environment which may contribute to failure after only a short working time. So, both mechanical resistance at high temperature and hot corrosion resistance are generally required simultaneously. In some situations, a single change in chemical composition is able to progress on the two ways simultaneously. This is the case with the introduction of hafnium in the chemical composition.

Hafnium is first known to significantly influence the oxidation behavior of high temperature oxidation of refractory materials of various types, ceramic as well as metallic [1–3]. For this reason, Hf is therefore added in some Nb–based alloys [4–6], Co–based alloys [7], Ni–alloys [8] or nickel aluminides [9–10]. Other uses of hafnium, general in higher quantities than in the previous cases, aim to develop HfC carbides in Co–based [11] or Ni–based [12] alloys for strengthening purpose for resisting stresses and creep at high temperature. Beside this mechanical aspect of HfC uses, the oxidation behaviors of materials rich in these carbides at high temperature were also investigated recently [13–15]. Since Hf is able to form MC carbides when it is present alone, its addition in replacement of the equivalent quantity of tantalum in a superalloy designed to be reinforced by MC carbides may possibly maintain the MC carbides network when, at the same time, it may improve the oxidation resistance at high temperature.

This is such a rather limited Ta–by–Hf replacement which was tested in this work. The initial chemical composition of a Ni–based alloy, designed to contain tantalum carbides by rating the molar fraction in Ta to make it equal to the molar fraction of carbon atoms, was modified to introduce 2 wt.% Hf instead of 2 wt.% of the initial 6 wt.% of tantalum. After elaboration by casting, the microstructure of the modified alloy was observed to possibly reveal a first effect on the as–cast microstructure. The benefits of this modification for the properties at high temperature were studied in term alloy surface stability during several tens of hours at three different high temperatures.

2. Experimental Details

2.1 The concerned alloy with partial replacement of Ta by Hf

The initial alloy was a Ni(bal.)–25Cr–0.4C–6Ta, all contents in weight percents. A previous study was devoted to the behavior in oxidation at high temperature of a series of alloys including this one [16]. It was noticed that this alloy was composed, in its as–cast state, of an austenitic matrix and of carbides of two types: TaC in majority, but also chromium carbides for a minor part. Its behavior in oxidation at elevated temperature was good (chromia–forming) but affected by a high tendency to oxide spallation at cooling, unfortunately.

The alloy which will be studied here derives from this previous alloy, with 2 wt.%Ta replaced by 2 wt.%Hf. As the previous one this alloy was synthesized by high frequency induction melting (110kHz, 5kV) under pure Argon (300mbars), with the same apparatus (CELES). The elements were introduced as pure metals (purity > 99.9%) and pure graphite. The supplier was Alfa Aesar. Its microstructure after its elaboration is illustrated in Fig. 1 in which one can see that it is constituted of a dendritic matrix and of interdendritic carbides of two kinds: the bright ones – major part – are MC carbides (M being Hf for the half, and Ta for the other half), and the dark ones are chromium carbides of the Cr_7C_3 type.

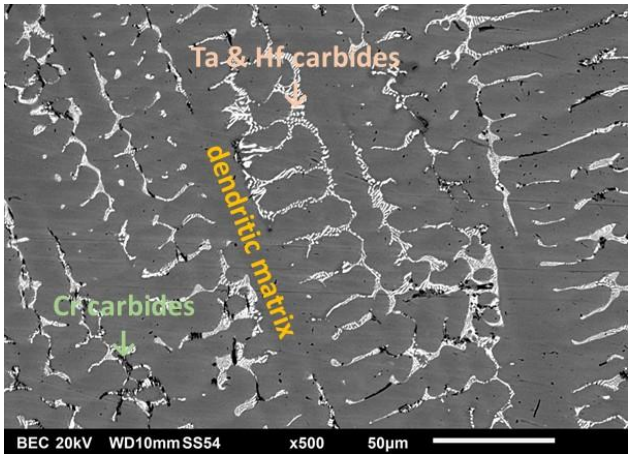

Figure 1. As–cast microstructure of the Ni–25Cr–4Ta–2Hf alloy**.**

2.2. Thermal analysis run

Considering the high levels of some of the oxidation temperature envisaged in this work, differential scanning calorimetry (DSC) was used to check whether the temperature of melting start of the studied alloy is well above 1250°C. The SETARAM TG–ATD 92 apparatus was used with a heating rate of 20°C/min up to 1200°C and of 5°C/min thereafter up to 1500°C (temperature range of interest) and a cooling rate of -5°C/min down to 1200°C (temperature range of interest) and -20°C/min thereafter to room temperature. The starts and end of heat absorption and heat release were noted to assess the solidus and liquidus temperatures of the alloy.

2.3. Oxidation tests

The obtained ingot was cut in order to have a part for the chemical and microstructure control of the alloy in his as–cast state, and to have three parallelepipeds to subject to high temperature oxidation tests. These latter parts were ground using SiC papers (#1200) on all their six faces. Edges and corners were themselves made rounder using the same papers (to avoid possible local overoxidation). The oxidation tests were carried out in a SETARAM TGA 92 thermo-balance with the following thermal cycles: heating at 20°C / minute, 50 hours isothermally spent at T, cooling at -5°C / min. T was 1100°C, 1200°C and 1250°C (three tests).

2.4. Metallographic analysis

The as–cast part of alloy and the three oxidized samples were examined by electron microscopy. The scanning electron microscope (SEM) JEOL JSM6010LA coupled with an energy dispersive spectrometer (EDS) was used using an acceleration voltage rated at 20kV (secondary electrons mode and back scattered electrons mode, respectively SE and BSE). Prior to these examinations X-ray diffraction (XRD) runs were done on the oxidized surfaces using a Bruker D8 Advance diffractometer, and a gold coating was created by cathodic evaporation over the oxidized samples to benefit from a high electrical conductivity for the SEM/SE observations of the oxidized surfaces. This also allowed depositing a thick electrolytic nickel shell all around them to allow cross–sectional cutting without loss of the external oxide scales, for the SEM/BSE and SEM/EDS characterization of the internal oxides and subsurfaces affected by oxidation.

3. Results and Discussion

3.1. Preliminary verification of the alloy's refractoriness

The DSC run performed of a part of the studied alloy led to the following estimated values: 1295°C for the solidus temperature and 1350°C for the liquidus temperature. By considering the solidus level, the choice of the maximum temperature (1250°C) was kept because of no risk of partial melting during the oxidation test at this temperature.

3.2. Oxidation kinetics at heating

The mass gain measures recorded in the numerical file correspond to four successive parts. The first one is the beginning of heating (low temperatures) during which the oxidation is extremely slow and cannot induce any measurable mass gain. The apparent mass variations revealed by the

microbalance present in the thermobalance were only due to the change in air buoyancy during heating. These variations were exploited to correct the measures from this phenomenon. This allowed thereafter to detect the real increase in mass of the sample by oxygen combination with some of the elements of the alloy. As soon as this mass gain by oxidation was detected the temperature was noted. This led to oxidation start temperatures globally ranging from 850 and 950°C for the three tests (Fig. 2). One must note that there is a lack of reproducibility concerning the temperature of oxidation start since the conditions of oxidation during the heating phase of the three tests are identical to one another between the ambient temperature and the neighbourhood of 1100°C (same alloy, same sample preparation, same apparatus, same heating rate). Since the two curves corresponding to 1200 and 1250°C are almost totally superposed and notably lead to the same oxidation start temperature, one can guess that there was a particularity for the sample corresponding to 1100°C. So, one can think that the real oxidation start temperature for this alloy is about 950°C.

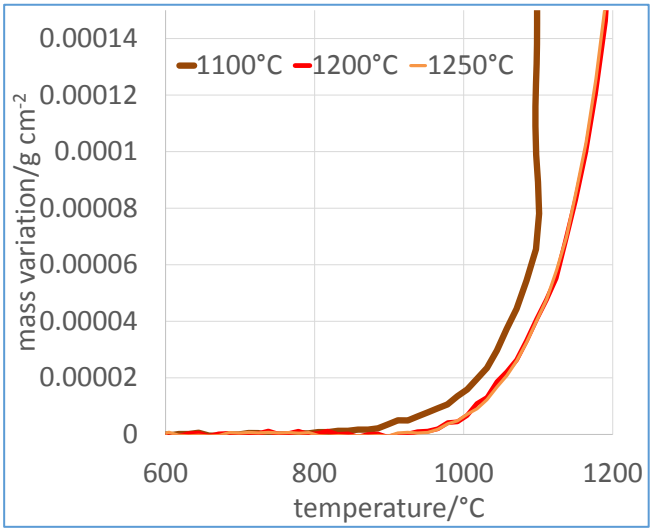

Figure 2. Heating: oxidation–induced mass variation of the alloy's sample, plotted versus temperature.

3.3. Oxidation in isothermal conditions

After exceeding the oxidation start temperature this is the second part of mass gain which started. It is characterized by a mass gain more and more rapid with the increase in temperature up to the one targeted for the isothermal stage. This isothermal stage constituted the third part of the mass gain (Fig. 3). For the three temperatures the isothermal mass gain kinetic was more and more fast for a temperature higher and higher. One can also observe that the kinetics are all parabolic. This suggested that, after a little transient time occurring just at the end of heating, the sample was uniformly covered by an oxide. Thereafter the progress of oxidation was governed by the diffusion of the species involved by oxidation through this continuous oxide scale, and obeys a Wagner's law: $m = (2 \times Kp)^{1/2} \times t^{1/2}$, where m is the mass per unit area (in mg / cm²) due to oxidation and t is time, both counted from the beginning of the isothermal stage, and Kp is the parabolic constant. This constant may be estimated by calculating $m_f^2 / (2 \times \Delta t)$, in which mf is the final mass gain measured by the thermobalance at the end of the isothermal stage, and Δt is the stage duration. However, since the continuous oxide scale separating the alloy from hot air is constituted of chromia (Cr_2O_3) – as this will be seen with the metallographic results – a phenomenon must be taken into account: the re–oxidation of chromia into gaseous CrO_3. The formation of this volatile oxide may be responsible of an underestimation of the mass gain kinetic, notably of the parabolic constant. So, before calculating Kp it is necessary to add, to the value of mf given by the microbalance, the mass loss which corresponds to the volatilization of a part of the chromia which formed. This mass loss can be calculated from the values of a volatilization constant Kv previously obtained for other chromia–forming alloys, simply by adding the value of $Kv \times \Delta t$. The Kv values which were used here for this correction of mf are the ones obtained earlier for a Ni–30Cr alloy at 1100°C and 1200°C [17]. For 1250°C no such Kv value was available and a tentative value was obtained by exploiting the fact that Kv obeys an Arrhenius law with an activation energy earlier estimated at 104 kJ / mol [17].

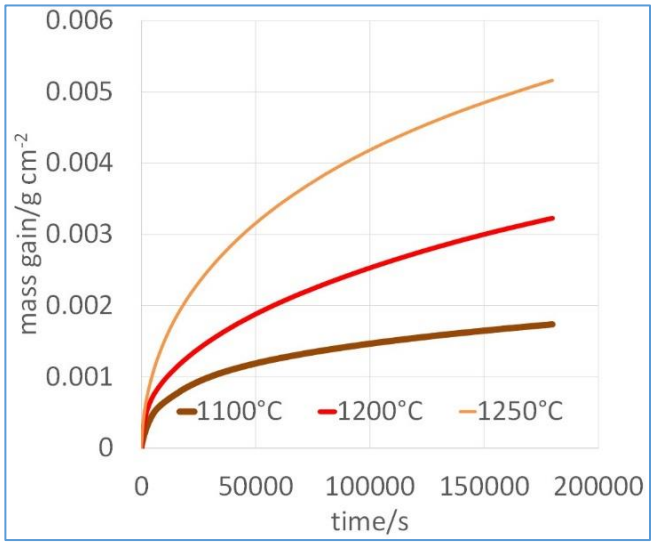

Figure 3. Isothermal stage: oxidation–induced mass variation of the alloy's sample, plotted versus time.

The obtained final mass gains and values of Kp are displayed in Table 1 and Table 2. This allows observing that the isothermal mass gains at the three test temperatures of the studied alloy are faster than for a Ni–30Cr ($Kp = 31 \times 10^{-6}$ mg² cm⁻⁴ s⁻¹ and 109×10^{-6} mg² cm⁻⁴ s⁻¹ against 23 × 10-6 mg² cm⁻⁴ s⁻¹ and 67×10^{-6} mg² cm⁻⁴ s⁻¹ for the Ni–30Cr alloy at 1100°C and

1200°C respectively [17]). The Kp differences with the reference Ni–30Cr alloy may be due to the oxidation of the Ta and Hf elements in addition to the one of chromium. Indeed, tantalum and hafnium are particularly reactive with oxygen. The post–mortem characterization of the oxide states will probably show the presence of many oxides of tantalum and of hafnium.

Table 1. Mass data resulting from the exploitation of the isothermal mass gain curves

Temperature	mass gain after 50h (m_f) (mg/cm²)	m_f corrected from chromia volatilization ($m_f + Kv \times \Delta t$) (mg/cm²)
1250°C	5.20	9.20
1200°C	3.25	6.27
1100°C	1.75	3.35

Table 2. Kinetic data resulting from the exploitation of the isothermal mass gain curves.

Temperature	Kp corrected from chromia volatilization $(m+Kv\times\Delta t)^2 / (2\times\Delta t)$ ($\times 10^{-6}$ mg² cm^{-4} s^{-1})	Kv values which were used for the Kp_{corr} calculations ($\times 10^{-7}$ mg cm^{-2}/s)
1250°C	235	222*
1200°C	109	168
1100°C	31.2	89

*: determined using an activation energy equal to 104kJ mol^{-1})

3.4. Behavior of the formed scales at cooling

The last parts of the mass gain curves may bring information about the stability of the oxidized surfaces during the cooling. This is of importance since cooling necessarily induces the appearance and the increase of compressive stresses in the external oxide scales, because of the lower thermal contraction of oxides than the one of alloys (average thermal expansion coefficient of oxides between two times and three times lower than the metals and alloys ones). In case of loss – partial or even total – of the external oxide scale at cooling, the alloys must thereafter reconstruct their protective continuous oxide scale during re–heating and isothermal exposure to hot gases, with as result an impoverishment in chromium of the subsurface which can threaten the sustainability of the chromia–forming behavior.

When plotted versus time, the examination of these cooling parts of the mass variation curves allows whether the oxide may spall off during the cooling, as well as, in the affirmative way, both the cooling time before the start of oxide spallation and the amount of the induced loss. When plotted versus temperature, as done just before for the heating phase (Fig. 2), one may directly know at which temperature the spallation phenomenon started. The mass variation curves during cooling plotted versus temperature are plotted together in Fig. 4. This allows seeing that the -5°C/min cooling which took over from the {1100°C, 50h}–isothermal stage induced no oxide loss. In contrast, oxide spallation obviously happened during the cooling after each of the two other oxidation tests. For the oxidation test at 1200°C, the first parts of oxides were lost when the temperature reached about 700°C, as is to say after 500°C of cooling. For this sample, the cooling from 700°C down to ambient temperature was continuously accompanied by a ceaseless irregular mass loss. At its return to room temperature, instead of a mass gain due to oxygen fixed on the sample as oxides, this is on the contrary a loss of mass which resulted from the whole test (about 6mg lost by cm^2), due to the loss of the greatest part of oxygen gained during the isothermal stage and the loss of a part of the chromium initially present in the sample subsurface and now present as lost Cr_2O_3 oxides. The mass loss is much greater for the sample oxidized at 1250°C. The spallation phenomenon, which started at about 800°C (i.e. 450°C below the isothermal stage temperature) led to close to 20mg of oxide lost per cm^2 (total final mass variation all around the thermal cycle: -13mg / cm^2). Obviously, for a given cooling rate, oxide spallation is favored by thick chromia scale and is an increasing function of this scale thickness.

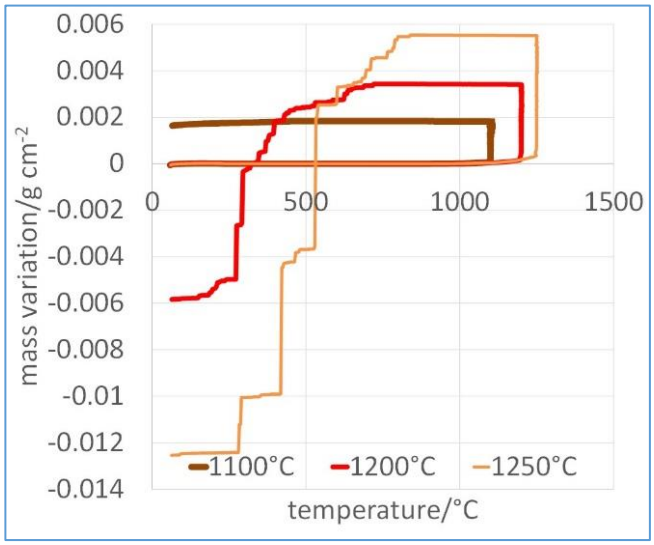

Figure 4. Cooling: oxidation–induced mass variation of the alloy's sample, plotted versus temperature.

3.5. Characterization of oxidized surfaces

After the thermogravimetry runs, the oxidized samples were carefully removed from the suspension system. XRD was performed on the oxidized surfaces of the three samples. The results, summarized in Fig. 5, show that the alloy behaved as a chromia–forming

alloy in all cases as demonstrated by the presence of Cr_2O_3 peaks in the three diffractograms. Chromia is particularly present over the sample oxidized at 1100°C (which did not know oxide spallation at cooling) while this is the mixed oxide $CrTaO_4$ (as well as the alloy, "fcc Ni") which is particularly detected for the two other samples which were severely affected by oxide spallation at cooling.

After gold deposition over the oxidized surface (thus become electrically conductive) the oxidized surfaces were examined by electron microscopy (prior to cutting for obtained cross–sections). Electron images taken in Secondary Electrons mode (SE) and in Back Scattered Electrons mode (BSE) illustrate the oxidized surface states in Fig. 6 and Fig. 7 respectively.

They evidence the continuous chromia scale covering the sample oxidized at 1100°C and the partly spalled external chromia scale still present of the surface of the sample oxidized at 1200°C. The denuded areas of this latter sample (oxidized 1200°C) are covered by the subjacent $CrTaO_4$ layer, while this mixed oxide of chromium and tantalum is present only as islands over the surface of the sample oxidized at 1250°C. For this latter sample, the alloy itself is visible: it represents the major part of the surface, this illustrating the very intense spallation phenomenon which occurred during the cooling.

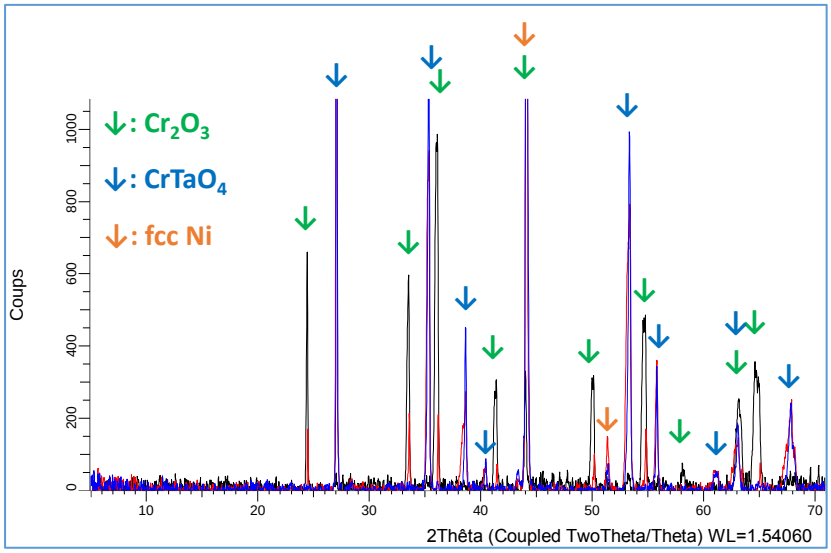

Figure 5. X–ray diffractograms of the sample's surface oxidized at 1100°C (black spectrum), 1200°C (red spectrum) and 1250°C (blue spectrum).

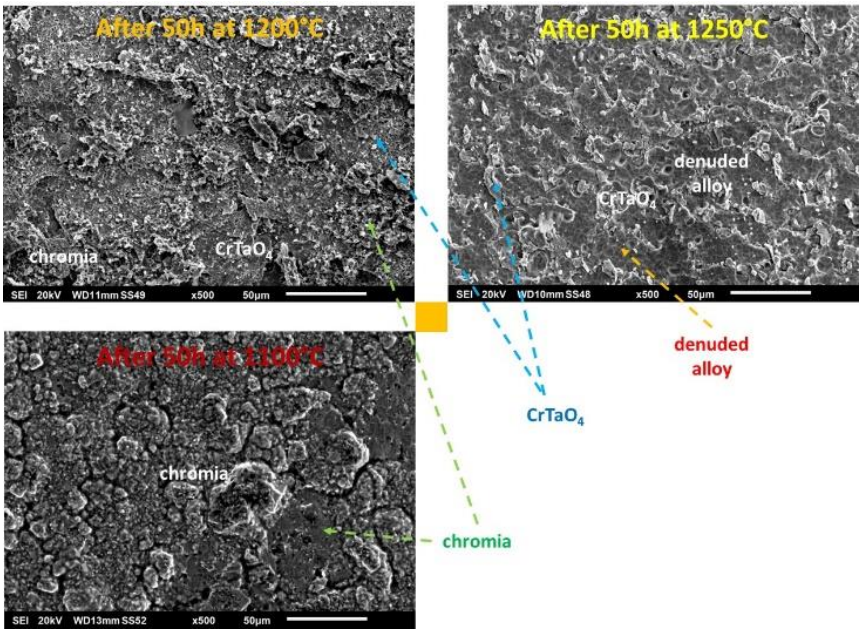

Figure 6. Post–mortem observations: SEM/SE micrographs taken on the oxidized surface prior to cross–sectional preparation.

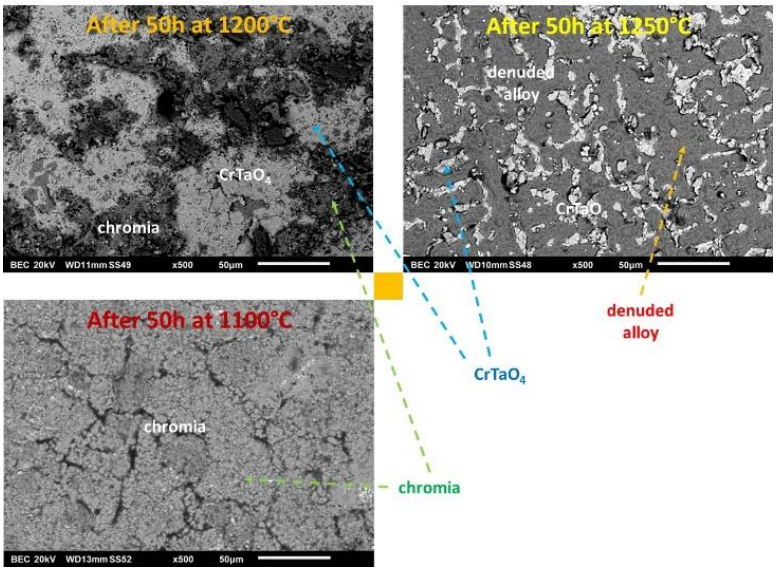

Figure 7. Post–mortem observations: SEM/BSE micrographs taken on the oxidized surface prior to cross–sectional preparation.

3.6. Cross–sectional observation of the external oxides, internal oxides and local microstructure changes

After cutting of the oxidized samples into two halves, embedding and polishing, the obtained cross–sections were observed with the SEM, in BSE mode. The thickness of the chromia scale formed over the surface of the sample oxidized at 1100°C (which is observable thanks to the absence of spallation at cooling and the careful metallographic preparation) seems to be about 10 µm (Fig. 8). Some porosities can be seen in this external oxide scale. Obviously internal oxidation also occurred, with the formation of $Cr(Ta,Hf)O_4$ islands in the subsurface, seemingly in the interdendritic boundaries. The depth of subsurface is of 20–25µm. Elemental X–maps acquired in the subsurface, presented in Fig. 9, complete the illustration of the subsurface oxide state: Cr_2O_3 on surface, and interdendritic $Cr(Ta,Hf)O_4$ in subsurface.

Fig. 10 (SEM/BSE subsurface views) and Fig. 11 (corresponding X–maps) illustrate the deteriorated state of the subsurface of the sample oxidized at 1200°C. Chromia is much less present (because of rather intense spallation at cooling) and the depth of subsurface affected by oxidation. The microstructure changes in subsurface are much visible: obviously, the primary (Ta,Hf)C carbides (appeared at solidification) have disappeared over a depth of about 100 µm while a curious secondary precipitation of fine (Ta,Hf)C carbides has occurred in a middle band in this subsurface zone of primary carbides disappearance. Closer to the surface one notices that blocky oxides of Ta and Hf have formed.

The oxidation–affected subsurface of the sample oxidized at 1250°C (Fig. 12 and Fig. 13) is particularly deep (150–200 µm).

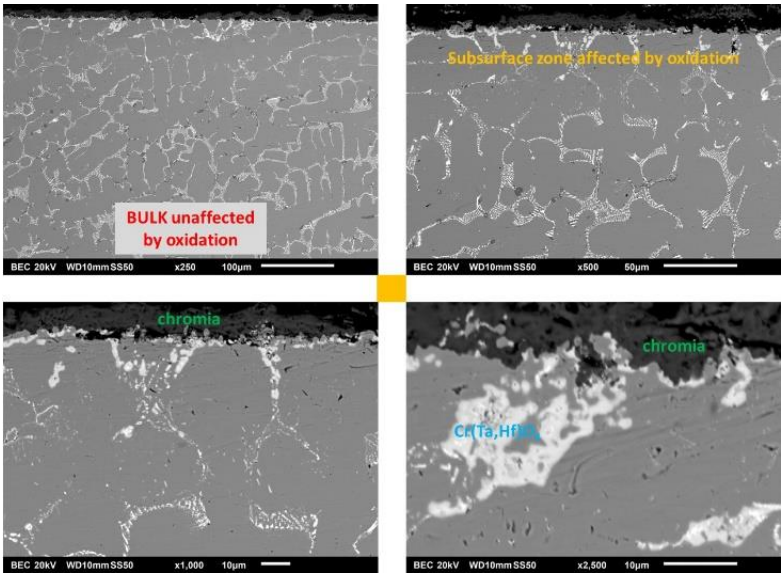

Figure 8. Post–mortem observations: SEM/BSE cross–sectional view at various magnifications of the subsurface of the sample oxidized at 1100°C.

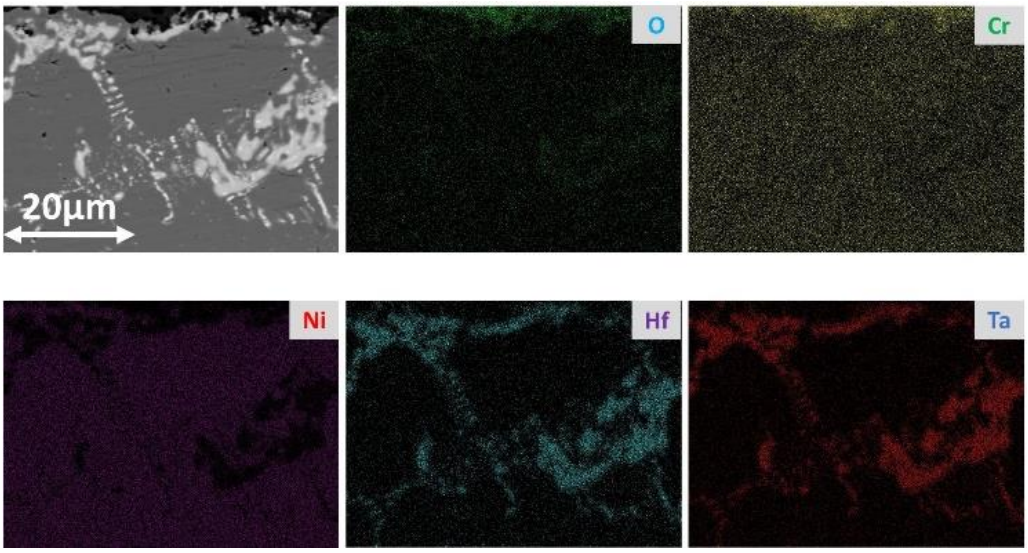

Figure 9. Post–mortem observations: SEM/BSE/EDS elemental mapping of the subsurface of the sample oxidized at 1100°C.

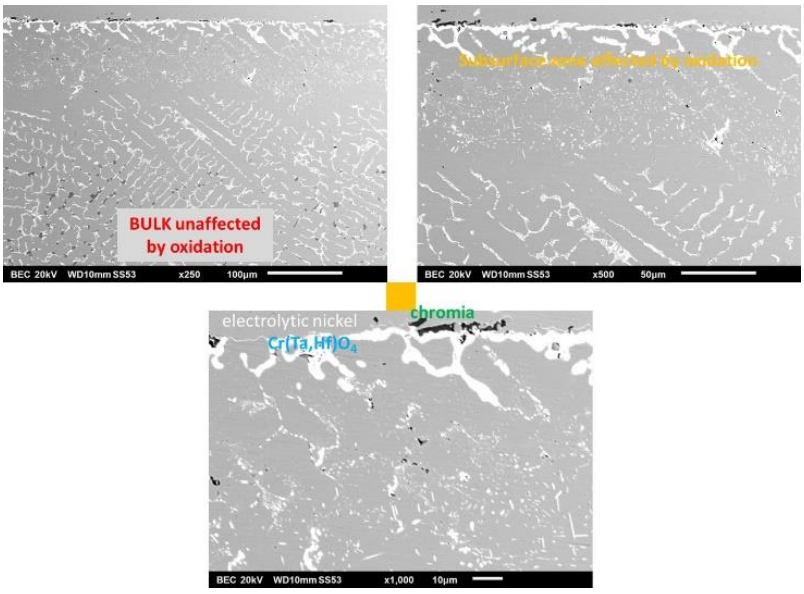

Figure 10. Post–mortem observations: SEM/BSE cross–sectional view at various magnifications of the surface and subsurface of the sample oxidized at 1200°C.

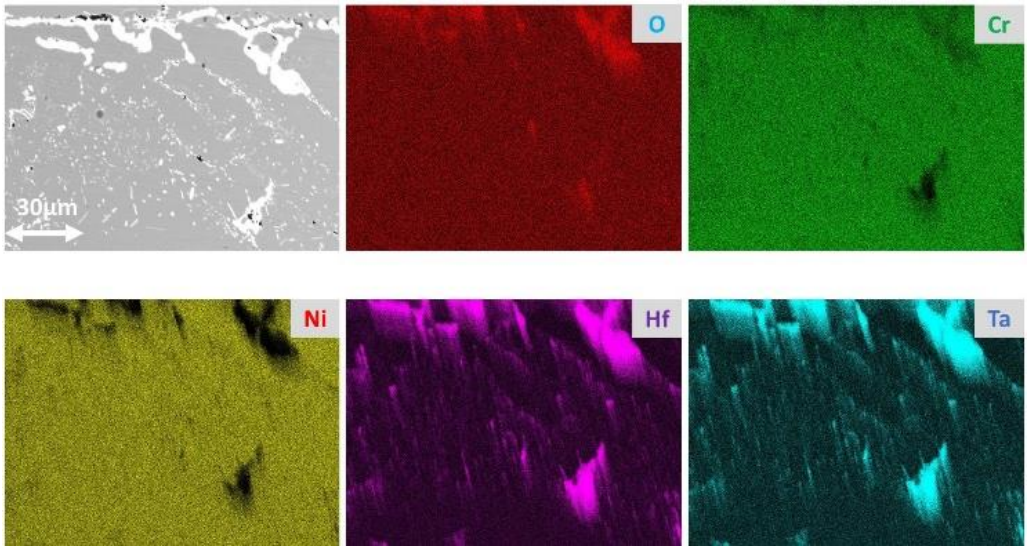

Figure 11. Post–mortem observations: SEM/BSE/EDS elemental mapping of the subsurface of the sample oxidized at 1200°C.

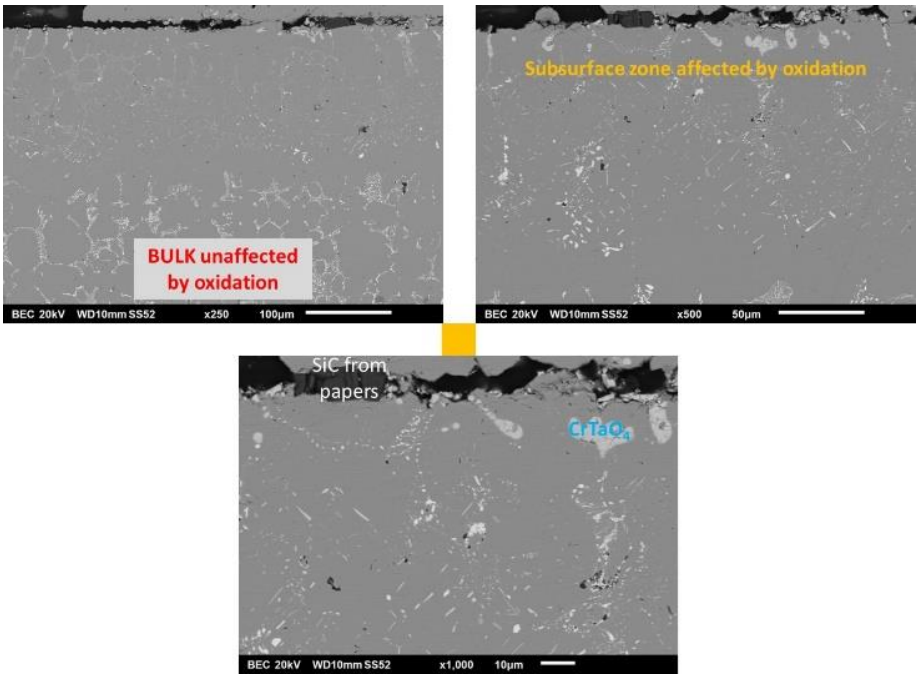

Figure 12. Post–mortem observations: SEM/BSE cross–sectional view at various magnifications of the surface and subsurface of the sample oxidized at 1250°C.

Here too, the initial interdendritic (Ta,Hf)C carbides have disappeared while fine secondary (Ta,Hf)C carbides have precipitated. Curiously the $Cr(Ta,Hf)O_4$ oxide seems to be less present: in fact one can easily imagine that the greatest part of this oxide was lost with the whole chromia scale during the very intense spallation at cooling. All the continuous and thick $Cr(Ta,Hf)O_4$ subjacent layer, the existence of which can be extrapolated from the observation of the subsurface states obtained at 1100 and 1200°C, fell down with the thick chromia scale, and only the internal part was kept.

3.7. Chemical changes in subsurface

The formation of oxides involving chromium, tantalum and hafnium necessarily induced a more or less severe impoverishment of the subsurface in these elements, with possible dangerous effects on the next oxidation resistance of the alloy. This is particularly true for chromium since, in case of decrease under a critical Cr content, the alloy may lose its chromia–forming behavior. This is the reason why about five spot EDS analyses were performed in the outermost alloy to know the local chemical composition after 50 hours of oxidation. The results are graphically presented in Fig. 14.

The average values and the error bars defined by the standard deviation values are plotted versus the temperature of the isothermal stage. It appears that, in extreme surface, the chromium content has decreased down to values which are functions of temperature: about 23wt.% for 1100°C, 21 wt.% for 1200°C and 20 wt.%Cr for 1250°C.

So, the higher the oxidation temperature, the lower the chromium content. However, even for 1250°C, the chromium content in extreme surface remains compatible with the sustainability of the chromia–forming behavior, since the alloy is based on nickel.

Concerning the other elements, only the content in tantalum has decreased. Unlike tantalum, hafnium seems being totally absent in the metallic part of the alloy (i.e. its matrix), whatever the state (as–cast or exposed at 1100, 1200 or 1250°C). This element seems being exclusively trapped in carbides or oxides formed in situ. When studied a little deeper, thanks to concentration profiles acquired from the extreme surface towards the bulk (Fig. 15), one can see that there are subsurface zones depleted in chromium and in tantalum.

The Cr depletion depth seems a little more extended than the Ta depleted ones, the latter corresponding more or less to the depths of disappearance of the primary (Ta,Hf)C carbides. The depths of the Cr and Ta depleted zones seems increasing with the isothermal oxidation temperature. Cr and Ta diffused easier and consequently from a deeper location when the exposure temperature was higher. At the same time, hafnium did not diffuse and stayed in the carbides.

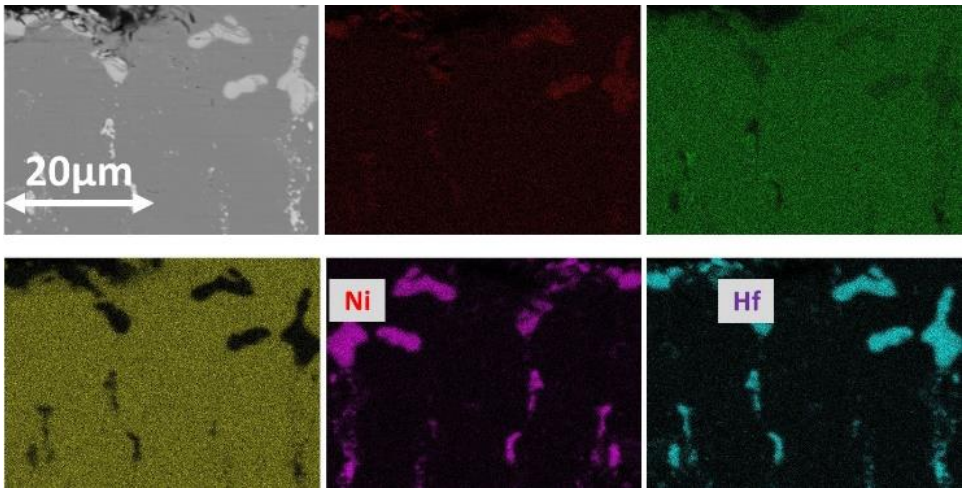

Figure 13. Post–mortem observations: SEM/BSE/EDS elemental mapping of the surface and subsurface of the sample oxidized at 1250°C.

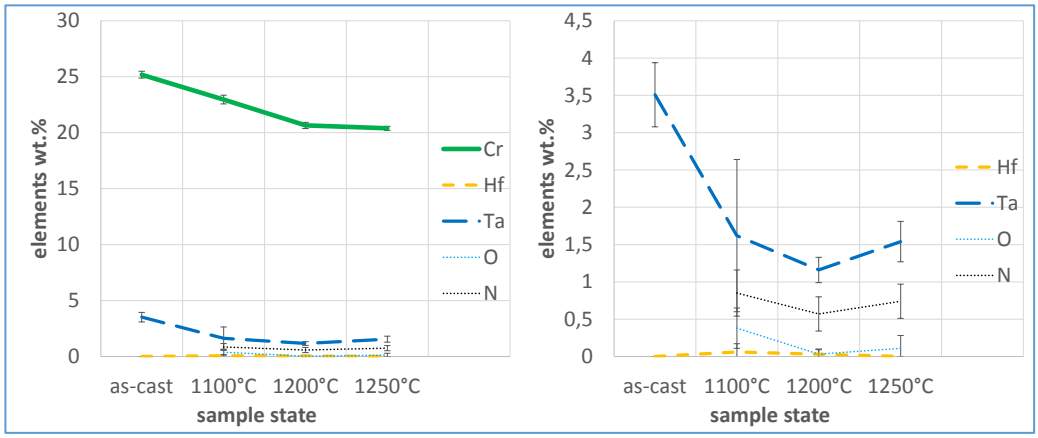

Figure 14. Composition of the extreme surface of the 50 hours–oxidized alloy in chromium (left) and in Hf and Ta (right) versus the oxidation temperature.

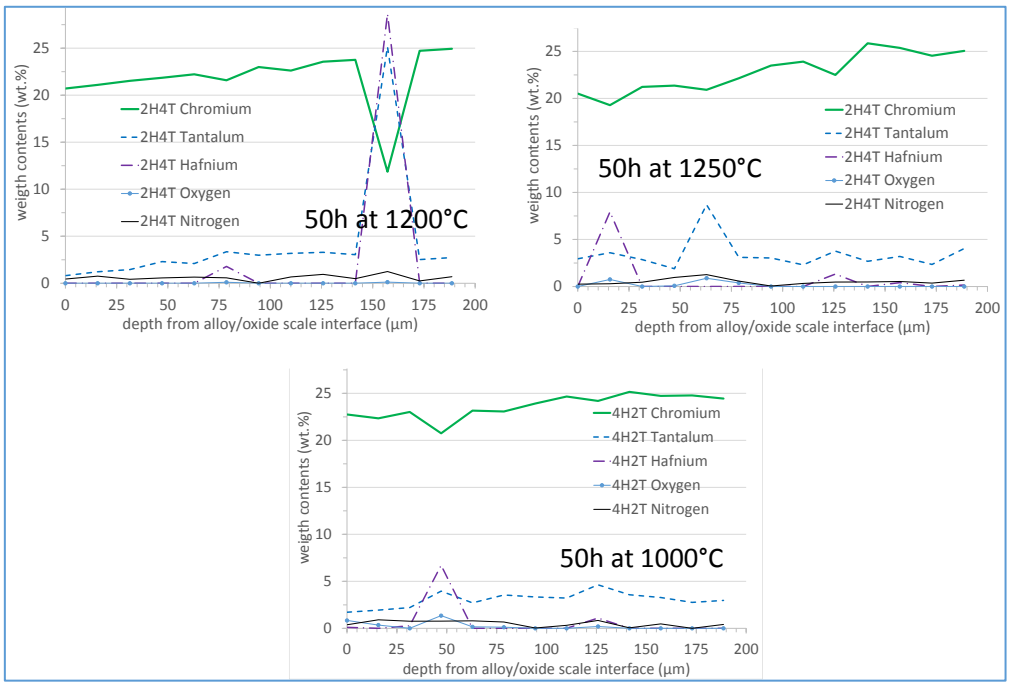

Figure 15. Profiles in subsurface concentration of the 50 hours–oxidized alloy in chromium (left) and in Hf and Ta (right) versus the oxidation temperature.

4. Conclusion

Hafnium is a very reactive element and its presence in a rather high concentration in the alloy considered here for having stable carbides was a possible reason of particular oxidation behavior of the alloy. Obviously, the alloy behaved in oxidation at elevated temperature rather well, even at 1250°C which represents an exceptionally high temperature for such type of alloys (polycrystalline, equi–axed, reinforced by carbides). Hf has showed that it is able to potentially improve the behavior of the strengthening by carbides (better stability in volume fraction and in morphology, than alloys containing only TaC) without detrimental effect on the oxidation resistance. The chromia–forming behavior is preserved and the subsurface deterioration is limited (less than 200 µm after 50 hours for the highest test temperature). The mass gain kinetic, a little increased consequently to a mass contribution of the oxidation of tantalum and hafnium in addition to the formation of chromia, stays close to the ones of other good chromia–forming alloys. The single oxidation problem is the tendency to oxide spallation when the chromia scale is thick, as obtained here after 50 hours of oxidation at 1200 or 1250°C. This may be a problem in industrial situation and this must be resolved, by yttrium addition for instance.

References

[1] L. Yang, H. Tang, G. Zhao, Effect of Hf and B incorporation on the SiOC precursor architecture and high-temperature oxidation behavior of SiHfBOC ceramics, Journal of the European Ceramic Society, 40(2) (2020) 324-332. [DOI]

[2] K. Yan, J. He, H-B. Guo, High-temperature oxidation behaviour of minor Hf-doped β-NiAl single crystals in dry and humid atmospheres, Rare Metals. 2018, Ahead of print. [DOI]

[3] E. Conrath, P. Berthod, Oxide spallation during post-isothermal high temperature oxidation cooling of Cr-rich cast alloys highly alloyed with Hf, Open Materials Science Journal, 10(1) (2016) 89-100. [DOI]

[4] I.G. Sharma, S. Majumdar, S.P. Chakraborty, A.K. Suri, Aluminothermic preparation of Hf–Ta and Nb–10Hf–1Ti alloys and their characterization, Journal of Alloys and Compounds, 350(1-2) (2003) 184-190. [DOI]

[5] R. Jiang, D. Liu, J. Sha, Y. Ma, High-temperature oxidation behavior of Nb67-xW15Si18Hfx(x=0, 5 and 10) alloys. Transactions of Nonferrous Metals Society of China, 16(3) (2006) 2009-2012.

[6] C.C. Wojcik, Properties and Heat Treatment of High Transition Temperature Ni-Ti-Hf Alloys, Journal of Materials Engineering and Performance, 18(5-6) (2009) 511-516. [DOI]

[7] F. Zhong, F. Fan, S. Li, J. Sha, High-temperature oxidation behaviour of novel Co-Al-W-Ta-B-(Mo, Hf, Nb) alloys with a coherent γ/γ'–dominant microstructure, Progress in Natural Science: Materials International, 26(6) (2016) 600-612. [DOI]

[8] D.A. Yancheshmeh, M. Esmailian, K. Shirvani, Microstructural and oxidation behavior of Ni-Cr-Al super alloy containing hafnium at high temperature, International Journal of Hydrogen Energy, 43(10) (2018) 5365-5373. [DOI]

[9] H. Guo, L. Sun, H. Li, S. Gong, High temperature oxidation behavior of hafnium modified NiAl bond coat in EB-PVD thermal barrier coating system, Thin Solid Films, 516(16) (2008) 5732-5735. [DOI]

[10] Y.Q. Wang, M. Suneson, G. Sayre, Synthesis of Hf-modified aluminide coatings on Ni-base superalloys, Surface and Coatings Technology, 206(6) (2011) 1218-1228. [DOI]

[11] P. Berthod, High temperature oxidation of cast cobalt-based alloys reinforced by different MC carbides (M = Ta, Nb, Hf or Zr). Annales de Chimie: Science des Materiaux, 34(5) (2009) 275-287.

[12] P. Berthod, Hafnium carbides in cast chromium-rich refractory alloys. Part 1: case of nickel-based alloys. Materials Science: An Indian Journal, 9(9) (2013) 359-365.

[13] L. Charpentier, M. Balat-Pichelin, D. Sciti, L. Silvestroni, High temperature oxidation of Zr- and Hf-carbides: Influence of matrix and sintering additive, Journal of the European Ceramic Society, 33(15-16) (2013) 2867-2878. [DOI]

[14] D.W. Lipke, S.V. Ushakov, Ultra-high temperature oxidation of a hafnium carbide-based solid solution ceramic composite, Corrosion Science, 80 (2014) 402-407. [DOI]

[15] C. Verdon, O. Szwedek, A. Allemand, S. Jacques, Y. Le Petitcorps, P. David, High temperature oxidation of two- and three-dimensional hafnium carbide and silicon carbide coatings, Journal of the European Ceramic Society, 34(4) (2014) 879-887. [DOI]

[16] P. Berthod, Microstructures and Surface Stabilities of {Ni-0.4C-6Ta-xCr, 0 ≤ x ≤ 50 Wt Pct} Cast Alloys at High Temperature, Metallurgical and Materials Transactions A, 49(6) (2018) 2311-2323. [DOI]

[17] P. Berthod, Kinetics of High Temperature Oxidation and Chromia Volatilization for a Binary Ni–Cr Alloy, Oxidation of Metals, 64(3-4) (2005) 235-252. [DOI]

Funding

No funding was received for conducting this study.

Acknowledgement

The Authors wish thanking the X-gamma centre of the Institut Jean Lamour.

Conflict of interest

The Authors has no conflicts of interest to declare that they are relevant to the content of this article.

Does the Article Screened for Similarity?

Yes.

About the License